Applied Catalysis B: Environmental 127 (2012) 265–272

Contents lists available at SciVerse ScienceDirect

Applied Catalysis B: Environmental

journal homepage: www.elsevier.com/locate/apcatb

Tungsten carbide on directly grown multiwalled carbon nanotube as a co-catalyst for methanol oxidation

Mansour Rahsepar[a,*], Mahmoud Pakshir[a], Pavel Nikolaev[b,1], Afsaneh Safavi[c], Kowsalya Palanisamy[b], Hasuck Kim[d,e]

[a] Department of Materials Science and Engineering, School of Engineering, Shiraz University, Zand Boulevard, Shiraz 7134851154, Iran
[b] Department of Energy Science, Sungkyunkwan University, 300 Cheoncheon-dong, Jangan-gu, Suwon 440-746, Republic of Korea
[c] Department of Chemistry, College of Sciences, Shiraz University, Shiraz 71454, Iran
[d] Department of Chemistry, Seoul National University, 599 Gwanak-ro, Gwanak-gu, Seoul 151-747, Republic of Korea
[e] Department of Energy Systems Engineering, Daegu Gyeongbuk Institute of Science & Technology, Daegu 711-873, Republic of Korea

ARTICLE INFO

Article history:
Received 14 July 2012
Received in revised form 20 August 2012
Accepted 28 August 2012
Available online 3 September 2012

Keywords:
Tungsten carbide
Carbon nanotubes
Fuel cell electrocatalysts, Methanol oxidation

ABSTRACT

Multiwalled carbon nanotubes (MWCNT) were grown directly on the surface of graphite rod by using CVD process and then modified with tungsten carbide by carbothermal hydrogen carbonization technique. Then, platinum nanoparticles were deposited on the MWCNTs by means of electrodeposition technique. Catalyst materials were characterized by electron microscopy, X-ray photoelectron spectroscopy and three electrode electrochemical measurements. Catalysts supported on the directly grown MWCNTs exhibit notably better electrocatalytic performance towards methanol oxidation compared to the commercial Pt/C catalyst. Modification of MWCNTs with tungsten carbide was shown to further increase the catalyst performance. It is believed that the superior performance of catalysts prepared on the MWCNTs as catalyst support results mostly from the superior electrical contact and unique spatial configuration of the directly grown MWCNTs, while the positive effect of the tungsten carbide co-catalyst is mostly attributed to its improved resistance towards poisoning with the reaction intermediates produced during the methanol oxidation.

1. Introduction

Fuel cells are considered to be the next generation of power sources, as potentially more efficient and less polluting power sources in comparison with the conventional thermal engines [1–4]. Within the last few years, there has been an accelerated interest in polymer electrolyte membrane fuel cells (PEMFCs) as a promising power source for applications such as electric vehicles and portable electronic devices [5–10]. Direct methanol fuel cells (DMFCs), using renewable liquid methanol as a fuel have been considered to be a favorable option in terms of simple construction, compact design, high energy density, and efficient fuel usage [11]. To improve the performance of PEMFC, it is of great importance to develop the catalyst layers with good activity for fuel electro-oxidation. Currently, Pt–Ru bimetallic catalyst is the most effective anode electrocatalyst for DMFCs [12]. However, in addition to the limited supply and high cost of platinum and ruthenium which hinder the extensive commercialization of fuel cells, Pt–Ru catalyst remains highly susceptible to poisoning *via* adsorption of methanol oxidation intermediate products, necessitating high catalyst loadings in the anode [13]. Therefore, development of new alternative catalysts is necessary to reduce or replace the expensive Pt–Ru bimetallic catalyst [14]. In the last several years, considerable efforts have been made to increase the performance of catalyst materials. Lots of researches have been conducted exploring new catalyst materials including noble and non-noble metals. Development of new platinum-based catalysts such as Pt–Ru [15–18], Pt–Sn [19], Pt–Cu [5], Pt–Ag [20] and Pt–Au [21] Pt–Ni [22] has been proposed to increase the catalytic performance. Moreover, it has been reported that transition metal carbides have exhibited platinum like behavior for fuel cell reactions [23,24]. A number of papers have been reported on the surface science and electrochemical performance of transition metal carbides as alternative electrocatalysts. Among these, tungsten carbide has received considerable attention and has been proposed as one of the promising materials in various catalytic reactions in PEMFCs [12]. In the 1960s, Binder et al. [25] for the first time reported on the oxidation of hydrogen with tungsten carbide electrodes in H_2SO_4 solution. It has been reported that the catalytic activity of tungsten carbide is attributed to its platinum-like electronic state, which is induced by filling the d-band at the Fermi level of tungsten when alloyed with carbon [26,27]. Several

* Corresponding author. Tel.: +98 711 2307293; fax: +98 711 2307293.
E-mail address: mansour.rahsepar@gmail.com (M. Rahsepar).
[1] Present address: UES Inc. & Air Force Research Laboratory, Dayton, OH, USA.

0926-3373/$ – see front matter © 2012 Elsevier B.V. All rights reserved.
http://dx.doi.org/10.1016/j.apcatb.2012.08.032

studies have been conducted on the electrocatalytic performance of tungsten carbide for hydrogen electro-oxidation [6,13,28–30]. Moreover, some papers have been reported on the electrocatalytic activity of metal-containing tungsten carbides [31,32]. Although electrocatalytic activity of tungsten carbide for fuel cell applications is still low, the initial results show that the application of tungsten carbide as platinum co-catalyst or catalyst support can promote the catalytic performance in terms of activity, durability and poisoning effects [33–37]. Recently, carbon nanotubes (CNTs) have attracted an increasing attention as an effective catalyst support due to their unique properties such as high current carrying ability, chemical stability, thermal conductivity and mechanical strength [38–42]. Recent studies also show that the modification of CNTs with tungsten carbide could be an effective option to improve their performance as a catalyst support [14,43–49]. Several investigations have been conducted on studying the electrocatalytic properties of tungsten carbide decorated on the outside surface of CNTs [14,43,44]. It has been concluded that the synergistic effect between Pt nanoparticle and tungsten carbide, besides the structural effect of MWCNTs, could result in significant enhancement of the methanol electro-oxidation.

It has been recognized that CNTs grown directly on the electrode surface can provide close physical and thus superior electrical contact between the deposited catalyst particles and the external electrical circuit and also improving Pt utilization [45,50]. However, to the best of our knowledge there has been no report on synthesis of tungsten carbide on directly grown CNTs as a catalyst support for methanol oxidation. In this work, we report on the modification of directly grown CNTs with tungsten carbide and their application for methanol electro-oxidation.

2. Experimental

2.1. Synthesis of directly grown multiwalled carbon nanotubes modified with tungsten carbide

Multiwalled carbon nanotubes were synthesized directly on the tips of graphite rods (99.999%, Sigma–Aldrich, 3 mm in diameter) by using chemical vapor deposition (CVD) process. Prior to CVD, Fe catalyst layer was galvanostatically deposited on the flat tips of graphite rods from an aqueous solution containing 0.45 M $FeSO_4{\cdot}7H_2O$ and other additives. MWCNTs were subsequently grown on the graphite surface in a CVD system (Thermo, UK). CNTs were grown by flowing 110 sccm ethylene as carbon source, 500 sccm hydrogen and 300 sccm argon at 750 °C for 1 h at ambient pressure. The furnace was then cooled down to ambient temperature under Ar atmosphere.

Carbothermal hydrogen carbonization process was used for synthesis of tungsten carbide on directly grown MWCNTs. An aqueous solution of tungsten powder (99.9%, Sigma–Aldrich) in H_2O_2 was used as the tungsten source for synthesis of tungsten carbide. CNTs were first impregnated with tungsten precursor by drop casting a required amount of tungsten solution on the surface of directly grown MWCNTs. Then, prepared samples were inserted in a quartz tube furnace and the carbonization process was carried out by heat treatment of the samples under flowing of gaseous mixture of 200 sccm of hydrogen and 600 of Ar at 850 °C for 2.5 h. Finally, furnace was cooled down to ambient temperature under Ar atmosphere.

2.2. Synthesis and dispersion of Pt nanoparticles on the surface of MWCNT and WC/MWCNT electrodes

Pt nanoparticles were deposited on directly grown MWCNT and tungsten carbide modified directly grown MWCNT (WC/MWCNT) electrodes by potentiostatic pulse electrodeposition technique. An Autolab potentiostat/galvanostat (Model, PGSTAT-302N) was used for the electrochemical deposition of Pt nanoparticles. Before Pt nanoparticle deposition, the metallic Fe catalysts were electrochemically removed [51]. Electrochemical purification was performed by cycling the electrode potential from 0.6 to 1 V (*vs.* Ag/AgCl) at a scan rate of 100 mV s^{-1} for 100 cycles in 2 M HNO_3 aqueous solution. Also, electrodes were subjected to electrochemical activation, involving cycling the potential from −0.2 to 1 V (*vs.* Ag/AgCl) at 50 mV s^{-1} for 50 cycles in 2 M H_2SO_4 aqueous solution. Pt pulse deposition was performed in a solution containing 0.25 M H_2SO_4 and 1.5 mM Pt at room temperature. Platinum(IV) chloride (Aldrich) was used as metal precursor. In order to remove dissolved oxygen from the plating bath, it was purged by N_2 bubbling for 10 min and then blanketed with N_2 during the electrodeposition process. A platinum wire was used as the anode. Pulse electrodeposition of Pt nanoparticles was conducted by applying 75 cycles of repetitive potential pulses of −0.3 V (*vs.* Ag/AgCl) for 0.1 s and 0.0 V (*vs.* Ag/AgCl) for 0.25 s. Composition of the electrodes was subsequently measured by EDS analysis, with no Fe detected on the electrodes after electrochemical purification and Pt nanoparticle deposition. The Pt loading on the electrodes surfaces was determined by ICP measurements with a Bruker 820-MS Inductively Coupled Plasma Mass Spectrometer. The platinum loading was determined to be 0.053 mg cm^{-2}.

2.3. Characterization of the catalyst

Electron microscopy was used to investigate the morphology and structure of the synthesized MWCNTs and catalyst nanoparticles. Electron microscopy investigations were carried out with a SUPRA 55VP (Zeiss) field emission scanning electron microscope (FE-SEM). Raman study was performed by means of a Renishaw microRaman (RM1000-Invia) system equipped with 514.5 nm laser. The surface chemical composition of the catalysts was analyzed by X-ray photoelectron spectroscopy (XPS). The XPS experiments were performed with an UHV multipurpose surface analysis system (SIGMA PROBE, Thermo, UK) operating at base pressures of $<10^{-10}$ mbar. The photoelectron spectra were excited with an Al Kα (1486.6 eV) anode operating at a constant power of 100 W (15 kV and 6.7 mA). During the spectra acquisition, the constant analyzer energy (CAE) mode was employed at 30 eV pass energy and 0.1 eV step. Deconvolution and curve-fitting of the spectra were performed using the Avantage software.

2.4. Electrochemical measurements

Electrochemical experiments were carried out with a three-electrode cell system consisting of an Ag/AgCl (3.5 M KCl) reference electrode and a platinum wire as the counter electrode. All potentials reported in this paper are *vs.* this reference electrode. An Autolab potentiostat/galvanostat (Model, PGSTAT-302N) was used for the electrochemical measurements. Electrochemical activity of electrodes for methanol oxidation was measured in nitrogen saturated 1.0 M CH_3OH + 0.5 H_2SO_4 aqueous solution. The CO stripping experiments were performed in 0.5 M H_2SO_4 solution. CO adsorption was carried out with continuous CO bubbling for 20 min while the anode potential was controlled at −0.14 V (*vs.* Ag/AgCl). The solution was then purged with 99.9% pure nitrogen gas for 30 min to remove dissolved CO before the stripping test.

Fig. 1. SEM micrograph of directly grown multiwalled carbon nanotubes.

3. Results and discussion

3.1. Physicochemical characterization of the catalysts

Morphology and configuration of the prepared catalyst materials were evaluated by using electron microscopy. Fig. 1 shows FE-SEM micrographs of the MWCNTs grown directly on the tip of graphite rod. It was observed that graphite surface is uniformly covered with directly grown MWCNTs with satisfactory surface appearance. According to SEM observations, directly grown MWCNTs have bamboo-like morphology and open porous structure which improves electrolyte access to the active sites of catalyst by decreasing mass transport limitations. In addition, the open porous structure of MWCNTs improves the Pt catalyst utilization during electrodeposition process and consequently leads to satisfactory dispersion of the catalyst nanoparticles. MWCNTs were further characterized by Raman spectroscopy. The Raman spectrum of MWCNTs is presented in Fig. 2. The peak located at ~1590 cm^{-1} is assigned to G-band originating from the graphite-like in-plane mode (E_{2g} mode) of MWCNT. The second peak at ~1350 cm^{-1} is assigned to D-band which is associated with the A_{1g} mode resulting from the disordered graphite structure. Two more peaks can be observed at ~2700 cm^{-1} (G′-band) and ~2930 cm^{-1} (G + D band), respectively. Since the D-band feature only becomes active in the presence of disorder, the intensity ratio of D- and G-bands is useful in evaluation of the extent of defects in MWCNTs. The I_D/I_G intensity ratio of MWCNTs is 1.12, which reveals the presence of disorder in MWCNT structure, consistent with their bamboo-liked morphology. Since defects provide active sites for the uniform distribution of catalyst during the deposition process, the disorder is beneficial for the uniform distribution of Pt nanoparticles.

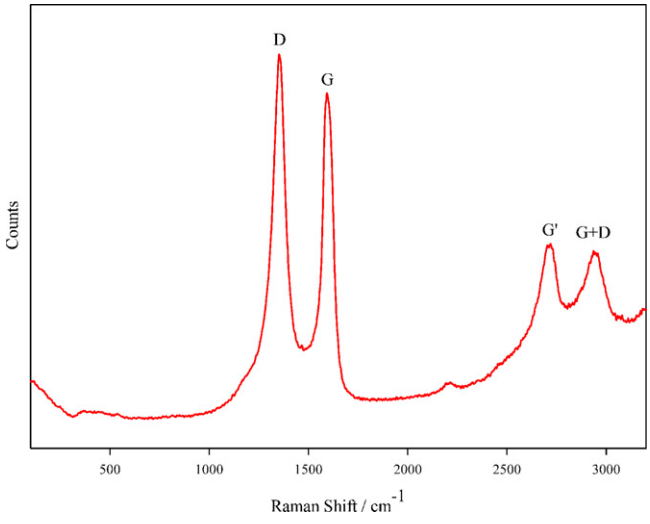

Fig. 2. Raman spectrum of directly grown MWCNTs.

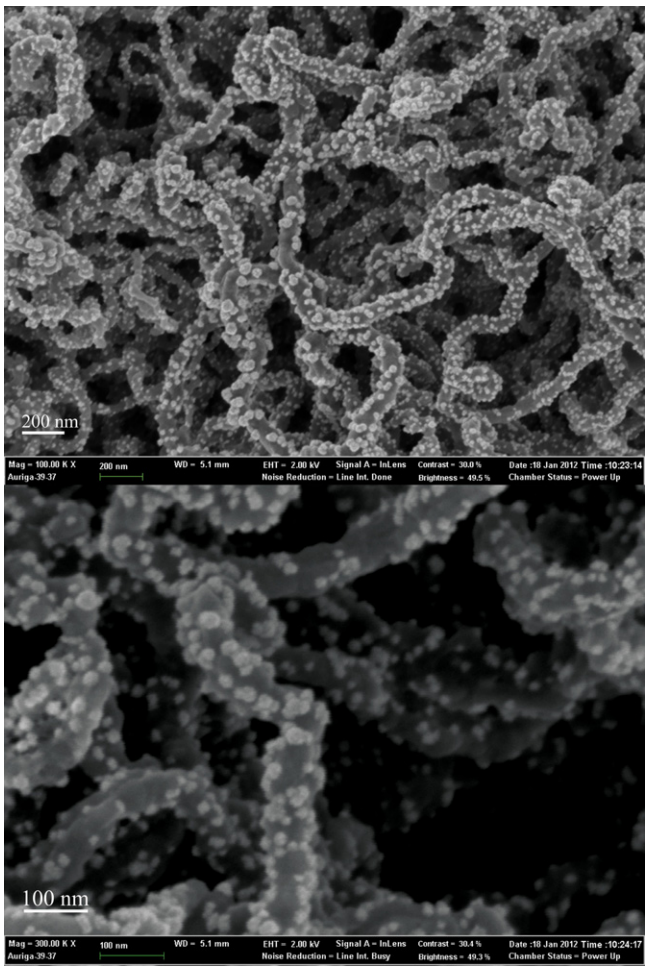

Fig. 3. SEM micrographs of the prepared Pt nanoparticles on directly grown multiwalled carbon nanotubes.

Pt nanoparticles were deposited on the surface of MWCNT and WC/MWCNT electrodes by potentiostatic pulse electrodeposition technique. SEM micrographs of Pt/MWCNT electrode catalysts are presented in Fig. 3. SEM micrographs show platinum nanoparticles that are uniformly distributed on the external surface of directly grown MWCNTs. SEM micrograph of Pt-WC/MWCNT electrode catalysts is presented in Fig. 4. It shows platinum nanoparticles that are uniformly distributed on the external surface of tungsten carbide modified MWCNT supporting materials. Moreover, one-dimensional nanostructure of MWCNTs was retained after carbonization process, and MWCNT exhibit a well-defined nanotube structure. The composition of electrodes was measured by using EDS analysis and no Fe was detected on the electrodes after electrochemical purification and deposition of Pt nanoparticles.

XPS analysis was used to study the surface chemical composition of catalyst materials. Initially, the surface composition of WC/MWCNT electrode was evaluated by the XPS survey scan. Only C 1s, O 1s and W 4f were detected on the surface of WC-MWCNT electrode. The chemical state of the tungsten was further studied by measuring the high resolution XPS of W 4f core level. The

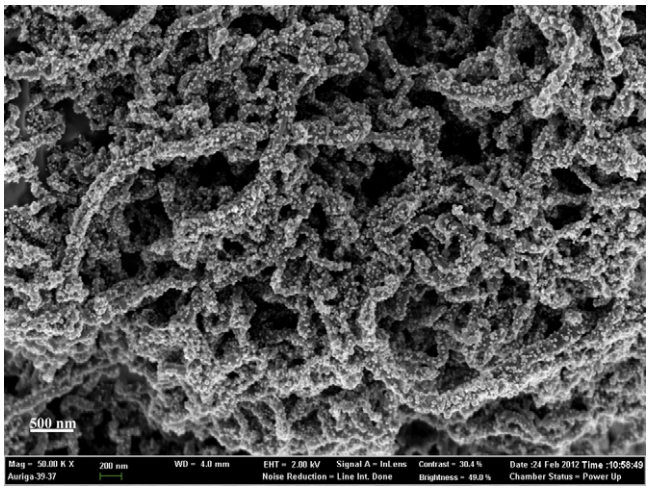

Fig. 4. SEM micrograph of the prepared Pt nanoparticles on tungsten carbide modified directly grown multiwalled carbon nanotubes.

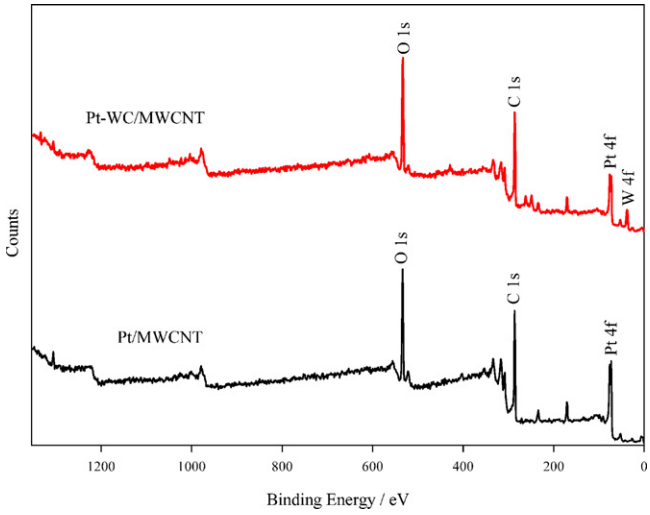

Fig. 6. XPS survey scan spectra of Pt/MWCNT and Pt-WC/MWCNT catalysts.

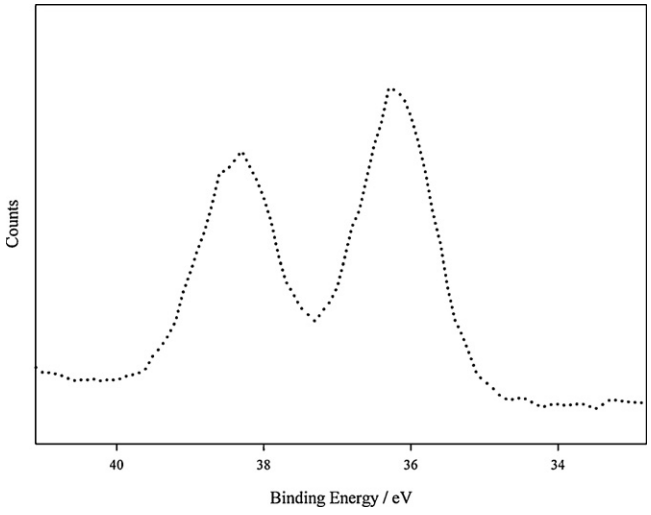

Fig. 7. High resolution W 4f XPS spectrum of Pt-WC/MWCNT catalyst.

corresponding results are presented in Fig. 5. It is observed that XPS signals of W 4f consist of four distinct features. As shown in Fig. 5, XPS peaks of W 4f core level can be deconvoluted into two doublets with bonding energies of 31.89–33.90 and 35.97–38.07 eV. The first doublet with 31.89 (W $4f_{7/2}$) and 33.90 eV (W $4f_{5/2}$) binding energies is assigned to the XPS signals of the tungsten carbide, while the second doublet with 35.97 (W $4f_{7/2}$) and 38.07 eV (W $4f_{5/2}$) binding energies is assigned to WO_3 [52–54]. While most tungsten presents in the sample surface is in form of carbide, there is a significant proportion of tungsten oxide, which possibly resulted from the electrode exposure to the atmosphere. Fig. 6 shows the XPS survey spectra of the Pt/MWCNT and Pt-WC/MWCNT catalysts. C 1s, O 1s, W 4f and Pt 4f peaks were detected on the surface of the Pt-WC/MWCNT electrode. High-resolution W 4f XPS spectra of the Pt-WC/MWCNT catalyst are presented in Fig. 7. XPS peak of the surface W 4f species are consisting of a doublet with 36.22 (W $4f_{7/2}$) and 38.32 eV (W $4f_{5/2}$) binding energies, which are assigned to tungsten oxide. Therefore, it is believed that the surface tungsten species that are beyond the detection limit of XPS analysis are oxidized to tungsten oxide during the electrochemical purification and activation process in acid solution.

The high resolution XPS spectra of Pt 4f of Pt/MWCNT and Pt-WC/MWCNT catalysts were analyzed as well to investigate the valence state of the platinum nanoparticles. As shown in Fig. 8, XPS peaks of Pt in both Pt/MWCNT and Pt-WC/MWCNT electrodes are a doublet consisting of Pt ($4f_{7/2}$) and Pt ($4f_{5/2}$) signals. The Pt 4f signal in both prepared catalysts shows a positive shift from the binding energies of the metallic Pt(0), which is attributed to the contribution of Pt(II) and Pt(IV) species [15]. The deconvolution of the Pt(0), Pt(II) and Pt(IV) species for both Pt/MWCNT and Pt-WC/MWCNT catalysts is shown in Fig. 8. The calculated binding energies and relative intensities are summarized in Table 1. Relative intensities of different species were calculated according to the areas of Pt $4f_{7/2}$.

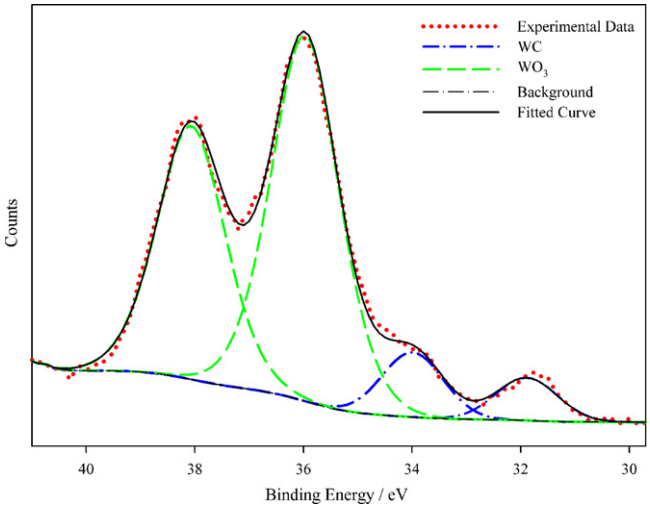

Fig. 5. High resolution W 4f XPS spectrum of WC/MWCNT.

Table 1
Binding energies and relative intensities of XPS spectra of Pt species in catalysts.

Catalyst	Species	Binding energy (eV)		Relative intensity (%)
		Pt $4f_{7/2}$	Pt $4f_{5/2}$	
Pt/MWCNT	Pt metal	71.63	75.01	35.97
	PtO	72.15	75.35	50.57
	PtO_2	74.46	77.4	13.46
Pt-WC/MWCNT	Pt metal	71.74	75.08	39.84
	PtO	72.23	75.68	50.09
	PtO_2	74.47	77.3	10.07

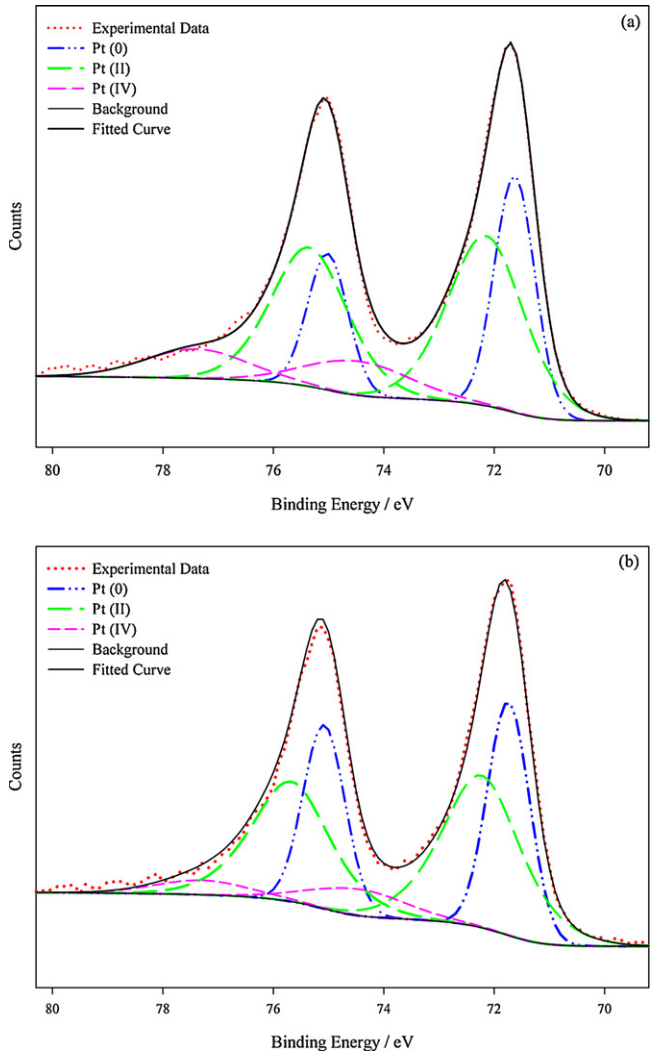

Fig. 8. High resolution Pt 4f XPS spectra of (a) Pt/MWCNT and (b) Pt-WC/MWCNT catalysts.

XPS results show that some platinum is present at the electrode surface in higher oxidation states.

3.2. Electrochemical performance

Electrocatalytic performance of the catalyst materials was studied using three electrode half cell measurements. Cyclic voltammograms of Pt/MWCNT and Pt-WC/MWCNT electrodes in a nitrogen-saturated 0.5 M H_2SO_4 are presented in Fig. 9. As shown in Fig. 9, cyclic voltammograms of both Pt/MWCNT and Pt-WC/MWCNT electrodes involve some features in the potential range of hydrogen adsorption (−0.2 to 0.10 V) in the cathodic direction which can be attributed to the hydrogen adsorption and reduction on the surface of platinum catalyst nanoparticles. Meanwhile, no well-defined peaks for quantitative analysis of the electroactive surface area are observed. Also a pair of broad redox peaks is observed between 0.2 and 0.45 V which is in agreements with that reported for Pt/MWCNT electrode in the literature [55,56]. These peaks originate possibly from the formation of carbonaceous functional groups and subsequent redox behavior of the carboxylic acid groups (such as –((COOH)ads and –((OH)ads) [55]. It seems that these broad peaks partially overlapped with hydrogen adsorption–desorption peaks and consequently make it impossible to calculate the electrochemically active surface area through the

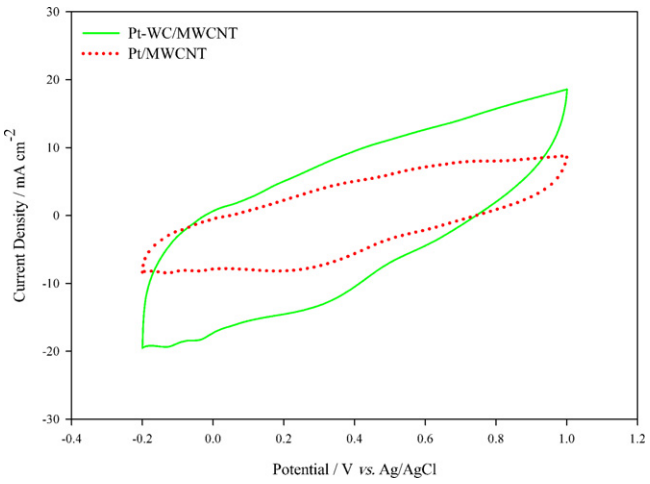

Fig. 9. Cyclic voltammograms of Pt/MWCNT and Pt-WC/MWCNT catalyst electrodes in 0.5 M H_2SO_4 aqueous solution; scan rate, 50 mV s^{-1}.

hydrogen adsorption–desorption features. On the other hand, as shown in Fig. 9, background voltammogram of the Pt-WC/MWCNT is larger compared with that of Pt/MWCNT electrode. Since the background is originated from the double-layer capacitance, it can be concluded qualitatively that Pt-WC/MWCNT electrode has a larger specific surface area [55,56].

Electrocatalytic performance of the electrodes toward methanol oxidation was studied by cyclic voltammetry of the electrodes in a nitrogen saturated 1 M CH_3OH aqueous solution containing 0.5 M H_2SO_4. Also cyclic voltammogram of methanol oxidation with commercially available 40 wt.% Pt/C (E-TEK) catalyst was used for comparison. In the case of commercial catalyst, the working electrode was a thin layer of Nafion bonded catalyst ink cast on a glassy carbon (3 mm in diameter) electrode; the fabrication procedure was described in detail elsewhere [15]. The Pt loading of the commercial catalyst electrode was ~0.226 mg cm^{-2} while that of both Pt-WC/MWCNT and Pt/MWCNT electrodes was ~0.053 mg cm^{-2}. Fig. 10 shows the cyclic voltammograms of different electrodes. Although the Pt loading of the commercial catalyst is about four times that of the prepared electrodes, the performance of the Pt-WC/MWCNT and Pt/MWCNT electrodes is better towards methanol oxidation, and both catalysts exhibit a lower peak potential for methanol oxidation. Since Pt loading of the prepared catalyst electrodes is different from that of the commercial Pt/C catalyst, specific current density was used to evaluate the electrocatalytic performance of the catalyst materials [56]. The specific current density is defined as the forward peak current density (mA cm^{-2}) per mg of Pt catalyst (mA cm^{-2} mg_{Pt}^{-1}). According to the cyclic voltammograms of methanol oxidation, the specific current densities of Pt/MWCNT and Pt-WC/MWCNT catalysts are 438.30 and 685.66 mA cm^{-2} mg_{Pt}^{-1}, respectively, while the specific current density of commercial Pt/C catalyst is 117.66 mA cm^{-2} mg_{Pt}^{-1}. It is believed that the superior performance of the prepared electrodes compared to the commercial Pt/C catalyst can be attributed to the physical nature of MWCNTs employed in this work as a supporting material. The directly grown MWCNT supporting materials on the substrate provide superior electrical contact between the catalyst particles and the external electrical circuit and also improve the utilization of Pt catalyst nanoparticles through their unique spatial configuration.

In addition, the specific current density of Pt-WC/MWCNT catalyst is 1.56 times as high as the specific current density of Pt/MWCNT catalyst. It can be concluded that modification of the directly grown MWCNTs with tungsten carbide leads to a significant improvement of the current density towards methanol

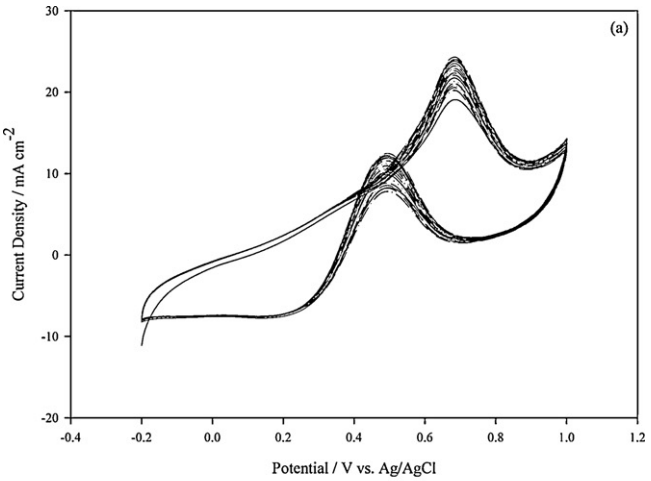

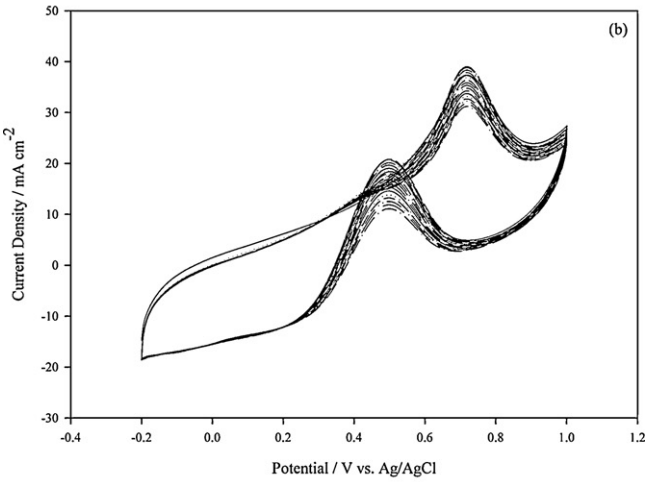

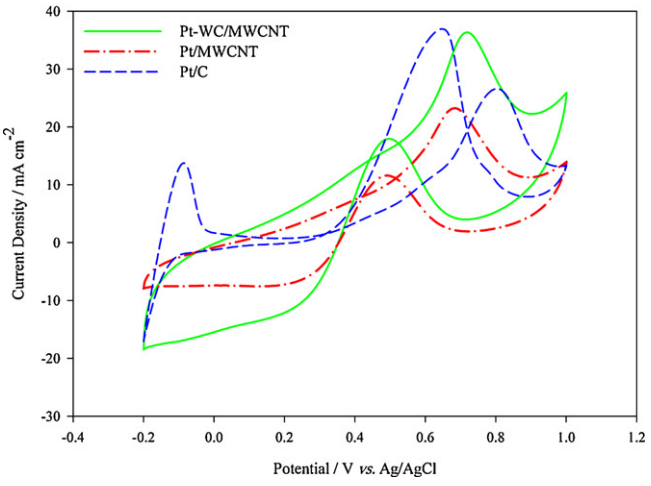

Fig. 10. Cyclic voltammograms of methanol oxidation on (a) Pt/MWCNT, (b) Pt-WC/MWCNT and (c) Pt/MWCNT, Pt-WC/MWCNT and Pt/C catalyst electrodes in 1.0 M CH_3OH + 0.5 M H_2SO_4 aqueous solution; scan rate, 50 mV s^{-1}.

oxidation compared to the Pt/MWCNT electrode. Methanol oxidation in acidic environment is a complex multi-step reaction, each step producing a variety of intermediate products. Some of these intermediate products are relatively stable compounds which strongly absorb on the catalyst active sites, leading to poisoning and dramatic loss of Pt catalytic activity. Effective catalyst for methanol

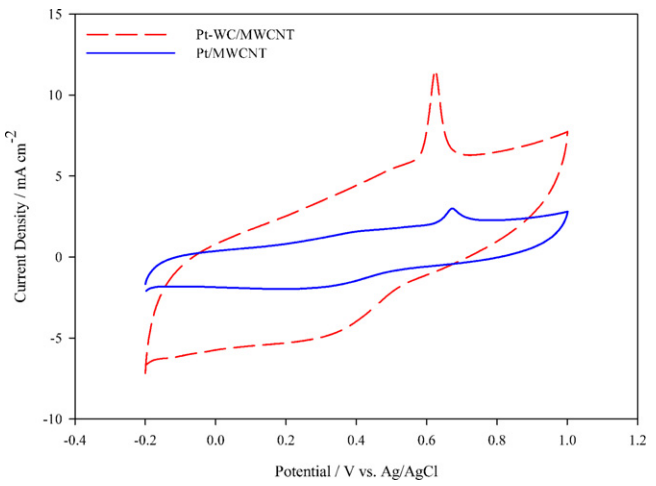

Fig. 11. CO stripping voltammograms of Pt/MWCNT (solid line) and Pt-WC/MWCNT (dotted line) catalyst electrodes in 0.5 M H_2SO_4 aqueous solution; scan rate, 20 mV s^{-1}.

oxidation must have good activity in promoting reaction of these intermediates with O-containing species to form CO_2. It has been reported that the tungsten carbide surface possesses higher activities towards water decomposition compared to Pt and Ru surfaces under similar conditions, and can provide O-containing species needed for these reactions [57]. Therefore higher activity of the Pt-WC/MWCNT electrode can be attributed to its higher resistance against poisoning by the methanol oxidation intermediates and thereby higher electroactive surface area is available for continuous oxidation of methanol.

To characterize the poisoning resistance of the prepared catalyst materials, CO stripping was carried out after cyclic voltammetry of methanol oxidation. Before CO stripping analysis, the electrode surface was electrochemically cleaned by potential cycling between −0.2 and 1 V for 20 cycles in 0.5 M H_2SO_4 solution. The CO stripping results are shown in Fig. 11. Pt-WC/MWCNT catalyst exhibited lower overpotential towards CO oxidation. It has been reported that the surface of W (1 1 1) carbide possesses lower CO desorption temperature compared with Pt and Ru surfaces under similar conditions [57]. Consequently, application of tungsten carbide as a co-catalyst for Pt can facilitate the oxidation and thus desorption of the absorbed CO and therefore improves the poisoning resistance of the catalyst material.

Finally, the steady state behavior of methanol oxidation on the surface of prepared catalysts was studied by chronoamperometric measurement at 0.7 V (*vs.* Ag/AgCl). Fig. 12 shows the results of chronoamperometric measurements of Pt-WC/MWCNT and Pt/MWCNT electrodes in 1.0 M CH_3OH aqueous solution containing 0.5 M H_2SO_4. Both electrodes reach a steady-state Faradic current response within approx. 200 s. It was observed that the tungsten carbide-modified MWCNT electrode produces a higher steady state current density in comparison with that of the unmodified electrode during the whole measurements. This could be attributed to the higher electrochemically active surface area of the tungsten carbides-modified electrode which is in agreement with the results of cyclic voltammetry of methanol oxidation. Meanwhile, decrease of steady state current density of the modified electrode within the first few seconds is lower compared to that of the unmodified electrode. Strong adsorbed intermediates from the methanol oxidation reaction and the corresponding poisoning action lead to the dramatic decrease of electrocatalytic activity of the platinum catalyst layer [12]. An effective anode electrocatalyst in direct methanol fuel cell (DMFC) should have both high activity for the oxidation of methanol and decomposition of water

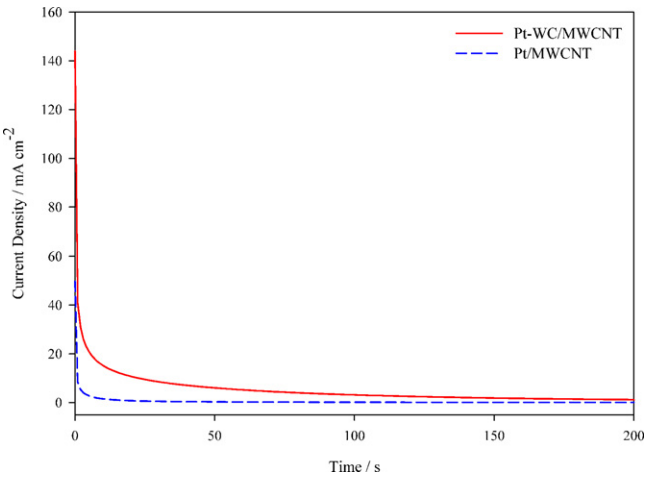

Fig. 12. Chronoamperograms of methanol oxidation on Pt/MWCNT and Pt-WC/MWCNT catalyst electrodes in 1.0 M CH_3OH + 0.5 M H_2SO_4 aqueous solution.

to remove intermediate products. However, the presence of tungsten carbide can significantly promote the electrocatalytic activity of the catalyst layer *via* the modification of reaction pathway and high performance of carbide phase as active sites for water decomposition reaction [12,53]. According to the mechanistic studies of the methanol oxidation on tungsten carbide, it has been reported that a fraction of methanol underwent a reaction pathway which produces the undesired gas-phase CH_4. However, modification of the C/W(1 1 1) and C/W(1 1 0) surfaces with low coverage of a Pt submonolayer would modify the methanol electro-oxidation pathway and eliminate the production of undesired products like CH_4 which reveals a synergistic effect between Pt and WC [12]. Thus, superior performance of the tungsten carbide modified electrode could be attributed to the synergistic effect of tungsten carbide on the electrocatalytic activity of platinum.

4. Conclusions

Multiwalled carbon nanotubes were directly grown on the surface of graphite rod by CVD process and were used as catalyst support for methanol oxidation. MWCNTs were modified with tungsten carbide as a platinum co-catalyst, followed by Pt catalyst nanoparticles deposition by electrochemical pulse deposition technique. Results of electrochemical measurements reveal that prepared catalysts show better electrocatalytic performance towards methanol oxidation compared to a commercial Pt/C catalyst with about 4 times higher Pt loading. It is believed that the superior performance of prepared electrodes is mostly attributed to the good electrical contact and unique spatial configuration of directly grown MWCNTs. Modification of MWCNTs with tungsten carbide further enhances the catalyst performance which is mostly due to the synergistic interaction between platinum and tungsten carbide and the ability of the tungsten carbide as a co-catalyst to facilitate the oxidation of methanol and the desorption of intermediate products formed during the methanol oxidation.

Acknowledgments

M.R. gratefully appreciates Seoul National University (SNU), Daegu Gyeongbuk Institute of Science & Technology (DIGIST, 11-BD-0405) and Sungkyunkwan University for research support in the form of research collaboration. M.R. also wishes to thank Ministry of Science, Research and Technology of Iran, Shiraz University and School of Engineering for their financial supports during his sabbatical stay in Korea. P.N. acknowledges support from the WCU program through the NRF of Korea, R31-2008-10029.

References

[1] Z.Q. Tian, S.P. Jiang, Y.M. Liang, P.K. Shen, Journal of Physical Chemistry B 110 (2006) 5343.
[2] C.Y. Wang, Chemical Reviews 104 (2004) 4727.
[3] A.L. Dicks, Journal of Power Sources 61 (1996) 113.
[4] S.S. Dihrab, K. Sopian, M.A. Alghoul, M.Y. Sulaiman, Renewable and Sustainable Energy Reviews 13 (2009) 1663.
[5] Z.D. Wei, Y.C. Feng, L. Li, M.J. Liao, Y. Fu, C.X. Sun, Z.G. Shao, P.K. Shen, Journal of Power Sources 180 (2008) 84.
[6] X.G. Yang, C.Y. Wang, Applied Physics Letters 86 (2005) 224104.
[7] K. Sundmacher, Industrial and Engineering Chemistry Research 49 (2010) 10159.
[8] C. Stone, A.E. Morrison, Solid State Ionics 152/153 (2002) 1.
[9] S.J.C. Cleghorn, X. Ren, T.E. Springer, M.S. Wilson, C. Zawodzinski, T.A. Zawodzinski, S. Gottesfeld, International Journal of Hydrogen Energy 229 (12) (1997) 1137.
[10] P. Costamagna, S. Srinivasan, Journal of Power Sources 102 (2001) 242.
[11] G.Q. Lu, C.Y. Wang, Journal of Power Sources 144 (2005) 141.
[12] E.C. Weigert, M.B. Zellner, A.L. Stottlemyer, J.G. Chen, Topics in Catalysis 46 (2007) 349.
[13] D.R. McIntyre, G.T. Burstein, A. Vossen, Journal of Power Sources 107 (2002) 67.
[14] Z. Zhao, X. Fang, Y. Li, Y. Wanga, P.K. Shen, F. Xie, X. Zhang, Electrochemistry Communications 11 (2006) 290.
[15] M. Rahsepar, M. Pakshir, Y. Piao, H. Kim, Electrochimica Acta 71 (2012) 246.
[16] A.L. Zhu, M.Y. Teo, S.A. Kulinich, Applied Catalysis A 352 (2009) 17.
[17] A. Rose, R. Bilsborrow, C.R. King, M.K. Ravikumar, Y. Qian, R.J.K. Wiltshire, E.M. Crabb, A.E. Russell, Electrochimica Acta 54 (2009) 5262.
[18] N.Y. Hsu, C.C. Chien, K.T. Jeng, Applied Catalysis B 84 (2008) 196.
[19] A.F. Innocente, A.C.D. Angelo, Journal of Power Sources 162 (2006) 151.
[20] V. Bansal, A.P. O'Mullane, S.K. Bhargava, Electrochemistry Communications 11 (2009) 1639.
[21] N. Kristian, X. Wang, Electrochemistry Communications 10 (2008) 12.
[22] Y. Hu, P. Wu, Y. Yin, H. Zhang, C. Cai, Applied Catalysis B 111/112 (2012) 208.
[23] S. Izhar, M. Nagai, Journal of Power Sources 182 (2008) 52.
[24] M. Rosenbaum, F. Zhao, M. Quaas, H. Wulff, U. Schroder, F. Scholz, Applied Catalysis B 74 (2007) 261.
[25] H. Binder, A. Kohling, W. Kuhn, W. Lindner, G. Sandstede, Nature 224 (1969) 1299.
[26] R.B. Levy, M. Boudart, Science 181 (4099) (1973) 547.
[27] L.H. Bennett, J.R. Cuthill, A.J. McAlister, N.E. Erickson, R.E. Watson, Science 187 (4179) (1975) 858.
[28] C.D.A. Brady, E.J. Rees, G.T. Burstein, Journal of Power Sources 179 (2008) 17.
[29] F. Harnisch, U. Schroder, M. Quaas, F. Scholz, Applied Catalysis B 87 (2009) 63.
[30] F. Harnisch, G. Sievers, U. Schroder, Applied Catalysis B 89 (2009) 455.
[31] M. Nagai, M. Yoshida, H. Tominaga, Electrochimica Acta 52 (2007) 5430.
[32] K. Lee, A. Ishihara, S. Mitsushima, N. Kamiya, K. Ot, Electrochimica Acta 49 (2004) 3479.
[33] M.B. Zellner, J.G. Chen, Catalysis Today 99 (2005) 299.
[34] F.P. Hu, P.K. Shen, Journal of Power Sources 173 (2007) 877.
[35] M. Nie, H. Tang, Z. Wei, S.P. Jiang, P.K. Shen, Electrochemistry Communications 9 (2007) 2375.
[36] Y. Wang, S. Song, V. Maragou, P.K. Shen, P. Tsiakaras, Applied Catalysis B 89 (2009) 223.
[37] N.R. Elezovic, B.M. Babic, P. Ercius, V.R. Radmilovic, L.M. Vracard, N.V. Krstajic, Applied Catalysis B 125 (2012) 390.
[38] P. Serp, M. Corrias, P. Kalck, Applied Catalysis A 253 (2003) 337.
[39] X. Wang, N. Li, J.A. Webb, L.D. Pfefferle, G.L. Hallera, Applied Catalysis B 101 (2010) 21.
[40] Y. Wang, X. Wang, C.M. Li, Applied Catalysis B 99 (2010) 229.
[41] S. Zhang, Y. Shao, G. Yin, Y. Lin, Applied Catalysis B 102 (2011) 372.
[42] E.O. Jardim, M. Goncalves, S. Rico-Francés, A. Sepúlveda-Escribano, J. Silvestre-Albero, Applied Catalysis B 113/114 (2012) 72.
[43] G. Li, C. Maa, J. Tang, J. Sheng, Electrochimica Acta 52 (2007) 2018.
[44] X. Shi, H. Yang, P. Sun, G. Shao, X. Duan, X. Zhen, Carbon 45 (2007) 1735.
[45] M.S. Saha, R. Li, X. Sun, S. Ye, Electrochemistry Communications 11 (2009) 438.
[46] P.H. Fernández, M. Montiel, P. Ocón, J.L. Gómez de la Fuente, S. García-Rodríguezc, S. Rojas, J.L.G. Fierro, Applied Catalysis B 99 (2010) 343.
[47] Z.M. Cui, S.P. Jiang, C.M. Li, Chemical Communications 47 (29) (2011) 8418.
[48] Z.M. Cui, C.M. Li, S.P. Jiang, Physical Chemistry Chemical Physics 13 (36) (2011) 16349.
[49] M. Rahsepar, M. Pakshir, Y. Piao, H. Kim, Fuel Cells, http://dx.doi.org/10.1002/fuce.201100202, in press.
[50] M.C. Tsai, T.K. Yeh, C.H. Tsai, Electrochemistry Communications 8 (2006) 1445.
[51] A. Heras, A. Colina, J. López-Palacios, P. Ayala, J. Sainio, V. Ruiz, E.I. Kauppinen, Electrochemistry Communications 11 (2009) 1535.

[52] E.C. Weigert, S. Arisetty, S.G. Advani, A.K. Prasad, J.G. Chen, Journal of New Materials for Electrochemical Systems 11 (2008) 243.
[53] V. Glibin, L. Svirko, I. Bashtan-Kandybovich, D. Karamanev, Surface Science 604 (2010) 500.
[54] A.L. Stottlemyer, E.C. Weigert, J.G. Chen, Industrial and Engineering Chemistry Research 50 (2011) 16.
[55] Z. He, J. Chen, D. Liu, H. Tang, W. Deng, Y. Kuang, Materials Chemistry and Physics 85 (2004) 396.
[56] H. Tang, J. Chen, S. Yao, L. Nie, Y. Kuang, Z. Huang, D. Wang, Z. Ren, Materials Chemistry and Physics 92 (2005) 548.
[57] H.H. Hwu, B.D. Polizzotti, J.G. Chen, Journal of Physical Chemistry B 105 (2001) 10045.